

Comment on ‘Detecting uniaxial single domain grains with a modified IRM technique’ by R. Mitra, L. Tauxe and J. S. Gee

K. Fabian

Geological Survey of Norway, 7491 Trondheim, Norway. E-mail: Karl.Fabian@NGU.NO

Accepted 2012 March 22. Received 2012 March 22; in original form 2011 December 23

SUMMARY

In a recent article, Mitra *et al.* (2011) propose a modified IRM technique to identify the symmetry of magnetic anisotropy in single domain particle ensembles. They apply this technique to support an earlier suggestion that single domain grains in young mid-ocean ridge basalts (MORB) exhibit multiaxial anisotropy. Here it is shown that the design of their measurement is flawed, in that they do not take into account that the outcome essentially depends on the initial demagnetization state of the sample before the experiment, and on the coercivity distribution of the sample. Because all MORB specimens measured by Mitra *et al.* (2011) carried their original NRM, which closely resembles a thermally demagnetized state, their measurements first of all reflect the coercivity distributions and domain states of the samples, and contain little or no information about the symmetry of the magnetic anisotropy. All arguments previously put forward in favour of a dominant uniaxial anisotropy in MORB are therefore still valid.

Key words: Magnetic fabrics and anisotropy; Magnetic mineralogy and petrology; Rock and mineral magnetism; Mid-ocean ridge processes.

1 INTRODUCTION

The predominant remanence carriers in mid-ocean ridge basalts (MORB) are titanomagnetite crystals $\text{Fe}_{3-x}\text{Ti}_x\text{O}_4$ with varying size and compositions near $x = 0.6$ (TM60) for young MORB's (Bleil & Petersen 1983; Matzka *et al.* 2003). Although the intrinsic crystal symmetry of titanomagnetite is cubic, titanomagnetites with high Ti content possess large magnetostriction constants, such that already minor internal stress of size $\sigma > 10$ MPa completely controls the magnetization directions, as has been confirmed by observations on synthetic and natural samples (e.g. Ambatiello & Soffel 1996). However, observations of high M_{rs}/M_s ratios, above the theoretical limit of 0.5 for prolate uniaxial anisotropy, have been interpreted in terms of prevailing cubic anisotropy in SD grains near the chilled margin of MORB samples (Gee & Kent 1995). In a previous study, Fabian (2006) collected several arguments which contradict this hypothesis:

(i) The high M_{rs}/M_s ratios are shown to be due to an underestimation of M_s when measuring hysteresis loops of high coercive TM60 in a maximum field of 1 T. Not a single sample shows $M_{rs}/M_s > 0.5$ when M_s is determined in fields of 5–7 T (Gee & Kent 1995; Matzka *et al.* 2003; Fabian 2006).

(ii) The effect of possible admixture of MD particles is corrected for by measuring seven specimens across a chilled margin and determining an independent grain size parameter $E_t^\Delta/E_{\text{hys}}$ for each. This parameter approaches zero for pure single domain particles and increases with grain size (Fabian 2003). By extrapolating the seven values of M_{rs}/M_s , measured at 7 T, to the limit $E_t^\Delta/E_{\text{hys}} = 0$, the

extrapolated single-domain value $M_{rs}/M_s = 0.48$ is obtained, which perfectly coincides with prolate uniaxial anisotropy.

(iii) The theoretical approach-to-saturation curve was modelled by minimizing the sum of anisotropy, stress and magnetostatic energy. Comparison of theoretical calculations for cubic anisotropy and stress induced anisotropy, to the measured upper hysteresis branch from MORB T787-R1 sample Xb12 close to the chilled margin clearly showed better coincidence with the stress dominated model.

(iv) Internal stress estimates from several studies on MORB yield values of at least 50 MPa, but typically around 200 MPa for young MORB.

(v) High M_{rs}/M_s ratios observed in synthetic TM60 are reduced by annealing. This indicates stress origin, because a predominance of cubic anisotropy would increase after internal stress is released by annealing.

The recent work of Mitra *et al.* (2011) does not strive to directly rebut the above results, but it seems to invalidate the arguments by contradiction in that Mitra *et al.* (2011) claim to provide independent proof for the presence of multi-axial single-domain particles in a set of MORB samples by using a new measurement procedure, especially developed for this purpose.

This proposed DIRM procedure essentially corresponds to a step-wise IRM-acquisition with the exception, that at every field step H two IRM values, $\text{IRM}^+(H)$ and $\text{IRM}^-(H)$, are measured, the first in $+z$ -direction, the other in $-z$ -direction. It is now observed that in some cases $|\text{IRM}^+(H)| \approx |\text{IRM}^-(H)|$, while in other cases clearly $|\text{IRM}^+(H)| > |\text{IRM}^-(H)|$. Mitra *et al.* (2011) quantify this finding

by introducing a ratio IRAT, which can be defined as

$$\text{IRAT}(H) = \frac{|\text{IRM}^-(H)|}{|\text{IRM}^+(H)|}. \quad (1)$$

They then put forward numerical calculations to demonstrate that $\text{IRAT} < 1$ is a clear indicator of multi-axial anisotropy, while $\text{IRAT} \approx 1$ signifies uniaxial anisotropy.

In the next section, it will be shown that any sample that has a sufficiently wide coercivity distribution can yield different DIRM results, because the outcome first of all depends on the initial state of the sample before the experiment. For thermally demagnetized initial states it will be shown that $\text{IRAT}(H)$ primarily reflects the domain-state and interaction dependent coercivity distribution in the sample with respect to H . Only for very well constrained single-domain particle ensembles the value of IRAT may in fact depend on the symmetry of the magnetic anisotropy. The MORB samples of Mitra *et al.* (2011) do not form such an ensemble.

2 PREISACH ANALYSIS OF THE DIRM TECHNIQUE

To show the strong influence of initial state and coercivity distribution, the DIRM measurement is most conveniently analysed by classical Preisach theory (Preisach 1935). Preisach theory is used in physics to model macroscopic magnetization processes (Bertotti 1998), and various versions and extensions are extensively studied in engineering and mathematics (Mayergoyz 1991; Visintin 1991). In rock magnetism, the Preisach model has been used to investigate interaction (Dunlop 1969; Dunlop *et al.* 1990), viscosity (Mullins & Tite 1973) and grain size (Ivanov *et al.* 1981). Experimentally determined Preisach functions yield detailed information about the coercivity distribution within natural samples (Hejda & Zelinka 1990). In the disguise of the FORC measurement scheme, initially developed by Girke (1960), mapping of the Preisach function is now routinely performed in rock magnetism (Pike *et al.* 1999, 2001).

Using the Preisach model it is also possible to understand the general theoretical relations between different magnetization processes (Fabian & von Dobeneck 1997). More advanced versions of Preisach theory (see e.g. Bertotti 1998) can take into account 3-D magnetization changes and thermal activation (Heslop *et al.* 2004), but this increases the complexity to a level not required for the argument here. In classical Preisach theory, any magnetic sample is represented by a collection of rectangular hysteresis loops (hysterons), characterized by their respective upwards and downwards switching fields (a, b) sketched in Fig. 1. The weight of the hysterons (a, b) are given by the Preisach function $p(a, b)$, which describes the sample. Concentrated Preisach functions along the line $a = -b$ describe single-domain ensembles, while broad maxima belong to PSD or MD ensembles (Ivanov *et al.* 1981). Whether a hysteron (a, b) is in *up* or *down* position depends on the initial state and the previous field history. When $p(a, b)$ and the *up-down* states of all hysterons (a, b) are known, the sample magnetization m can be calculated by

$$m = \int_{S^+} p(a, b) da db - \int_{S^-} p(a, b) da db, \quad (2)$$

where S^+ and S^- denote the regions of the a - b -plane where the hysterons are switched upwards (S^+), or downward (S^-), respectively.

To study the DIRM process, it is essential to follow the change of shape of these S^\pm -regions. Fig. 2 does this for two initial demagnetization states, an AF-demagnetized state in Fig. 2(a),

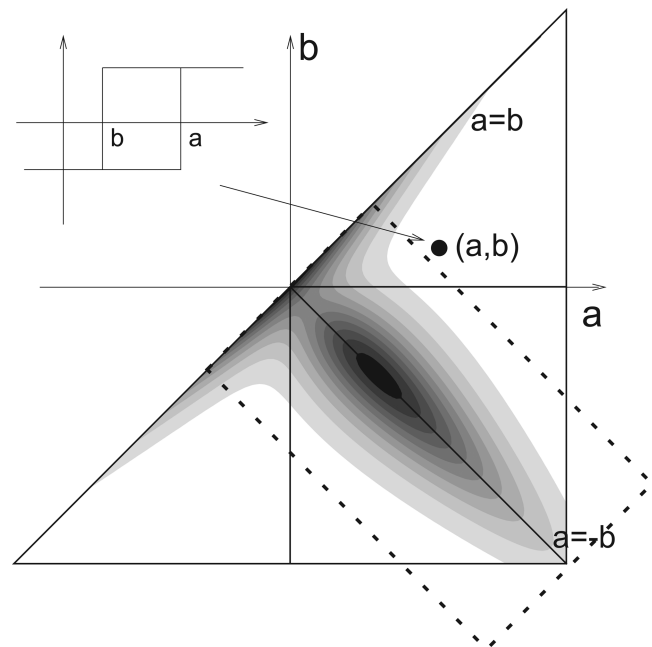


Figure 1. Sketch of the Preisach representation of isothermal magnetization processes. Each point in the $a - b$ -plane represents a rectangular hysteresis loop with switching fields $a \geq b$. The Preisach function $p(a, b) \geq 0$ indicates the weight of the (a, b) -loop within the sample. FORC diagrams $f(a, b)$ approximate the Preisach function and are usually represented in a 45° rotated coordinate system (dotted line). Ideal Preisach functions are symmetric with $p(a, b) = p(-b, a)$, which only approximately holds for $f(a, b)$. The shown Preisach function represents a typical natural sample containing pseudo-single domain particles, and resembles some FORC distributions of Mitra *et al.* (2011). For pure SD ensembles $p(a, b)$ is concentrated along the line $a = -b$, for MD ensembles it is much wider and closer to the line $a = b$.

and a thermally demagnetized state in Fig. 2(d). After AF-demagnetization in z -direction, each hysteron is in the state where its lowest switching field left it. Hysterons with $-b > a$ are in the *up* state, while those with $-b < a$ are in the *down* state. Due to the symmetry of $p(a, b)$, the total remanence in this state is $m = 0$. By applying a positive field H , and switching it off again, all hysterons with $a < H$ will first be switched in the *up* state, and those with $b > 0$ will then be switched back to their *down* state. The result is shown in Fig. 2(b). When calculating the magnetic moment of this state using eq. (2), one notices that the symmetric parts of S^+ and S^- cancel and the IRM can be simply represented by the integral over the area W bounded by the white dotted line in Fig. 2(b).

$$\text{IRM}_{\text{AF}}^+(H) = \int_W p(a, b) da db. \quad (3)$$

To model DIRM, one now has to apply the same field in the negative direction, switching all loops with $b > -H$ to *down*, and then all with $a < 0$ to *up* again. As seen in Fig. 2(c), the resulting S^\pm -regions are mirror symmetric to those in Fig. 2(b), such that $|\text{IRM}^+(H)| = |\text{IRM}^-(H)|$. This means that whatever sample is used, after AF-demagnetization in z -direction the measured value of IRAT will be constant and equal to 1.

In contrast, the thermally demagnetized state in Fig. 2(d) is achieved by statistically demagnetizing each hysteron. This means that exactly identical particles assume random *up-down* states, independent of their switching fields a and b . Starting from this initial state, the DIRM process in fact leads to a different result. After

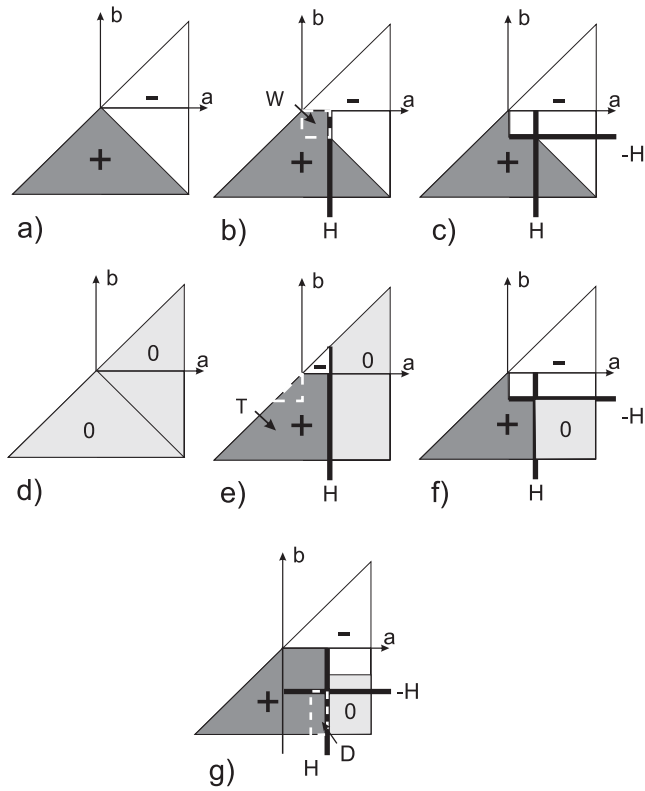


Figure 2. Preisach representation of the DIRM measurement starting from different initial states. Dark areas marked with ‘+’ represent the regions S^+ , where hysteron are in ‘up’ state, white areas marked with ‘-’ represent the regions S^- , where hysteron are in ‘down’ state. Light gray areas marked with ‘0’ represent thermally demagnetized hysteron contributing neither to S^+ , nor to S^- . (a) Initial state after AF-demagnetization in the z -direction. (b) IRM state after applying a positive field H following AF-demagnetization. (c) DIRM state after applying a negative field $-H$ following the IRM state in (b). (d) Initial state simulating thermal demagnetization. (e) IRM state after applying the first positive field H following state (d). (f) DIRM state after applying a negative IRM in field $-H$ following state (e). (g) DIRM state after applying an IRM in a higher positive field H following state (f) for a smaller field.

applying a positive field H , all hysteron with $a < H$ again will be switched in the ‘up’ state, and those with $a < H$ and $b > 0$ will be switched to the ‘down’ state (Fig. 2e). After cancelling the small symmetric regions with opposite magnetization, marked with a white dotted line in Fig. 2(e), the integral over the remaining positive region T yields

$$\text{IRM}_{\text{thermal}}^+(H) = \int_T p(a, b) da db. \quad (4)$$

Region T contains region W in Fig. 2(b), whereby $|\text{IRM}^+(H)|$ after thermal demagnetization is potentially larger. If now the same field is applied in the negative direction, all loops with $b > -H$ switch to ‘down’, and all with $b > -H$ and $a < 0$ switch to ‘up’ (Fig. 2f). Interestingly, the net moment predicted by these S^\pm -regions is exactly the same as for AF-demagnetization, resulting in $|\text{IRM}^+(H)| \geq |\text{IRM}^-(H)|$, or IRAT less or equal to 1. By proceeding further with the IRAT measurements, the situation in Fig. 2(e) is replaced by that in Fig. 2(g), because the previous application of a negative field switched all hysteron with $b > 0$ to their negative state. Accordingly, the region T of (4) in this case becomes $T =$

$W \cup D$, where D is indicated in Fig. 2(g). The relation $|\text{IRM}^+(H)| \geq |\text{IRM}^-(H)|$ remains valid.

3 DISCUSSION

The above Preisach analysis of the DIRM method predicts that the result of the experiment depends on the initial state of the sample, and on the coercivity distribution in relation to the measurement field steps. Both dependencies have not been considered by Mitra *et al.* (2011). Instead, they interpreted the value of IRAT solely in terms of single-domain magnetic anisotropy, based on numerical simulations.

Already these numerical calculations of Mitra *et al.* (2011) appear problematic considering the reported model values of M_{rs}/M_s . Whilst $M_{rs}/M_s = 0.5$ for a three dimensionally randomized uniaxial numerical SD ensemble agrees with theoretical calculations, the reported value of $M_{rs}/M_s = 0.94$ for hematite-like triaxial symmetry in the basal plane is much too high. For a three dimensionally randomized ensemble, M_{rs}/M_s in this case certainly should be lower than the theoretical value of $M_{rs}/M_s = 0.638$ for platelets. Only in case of SD hematite particles with perfectly aligned basal planes, and field direction within this plane a value of $M_{rs}/M_s = 0.94$ can be obtained. However, Mitra *et al.* (2011) explicitly state that they use randomly oriented grains. The last and maybe decisive reason why the numerical results are misleading is the choice of alternative models. Material constants for low coercive magnetite were chosen to represent uniaxial anisotropy, whilst high coercive hematite represents the multiaxial case. Due to the large field steps chosen in the model calculations (as well as in the experiments), the low coercive magnetite naturally shows IRAT close to 1, while the high-coercive hematite can exhibit lower values when starting from a random initial state, resembling the thermally demagnetized one. The model results may therefore just reflect a contrast of low and high coercive materials, while they are interpreted as being characteristic for uniaxial versus multiaxial magnetic anisotropy. It is conceded that multiaxial anisotropy may contribute to IRAT, but as pointed out by the above Preisach model calculations, a careful consideration of the coercivity distribution is required before possible multiaxial contributions can be identified. In simple terms, if a sample contains PSD particles along with SD particles, an interpretation of low IRAT solely in terms of multiaxial anisotropy is misleading.

A question that remains is why the diagram of M_{rs}/M_s versus IRAT for MORB specimens in fig. 10 of Mitra *et al.* (2011) shows a clear trend. The explanation has two parts. First, the DIRM measurements are performed on samples carrying their initial NRM. This NRM is a TRM acquired in a weak field, and—as pointed out by the authors—essentially represents a thermally demagnetized state. Therefore, in agreement with the Preisach calculation, the measured IRAT values can be less than 1. Secondly, considering the relatively large field steps used (50 mT, 100 mT, 200 mT, 300 mT, 400 mT, 500 mT), only samples with a considerable remanence, that is, $p(a, b)$ fraction, at these high coercivities can have low IRAT at these fields, because region D in Fig. 2(g) must contain some magnetization. The FORC distributions in fig. 6 of Mitra *et al.* (2011) show that this is best fulfilled for specimens close to the chilled margin, while those further inside have too low coercivity, and correspondingly display IRAT values close to 1. Due to their high coercivity, the low IRAT samples also display large M_{rs}/M_s , partly because of high remanence, and partly due to insufficient saturation and accordingly too low apparent M_s (Fabian 2006). This IRAT result, which most

likely just reflects the coercivity distributions, is solely interpreted in terms of anisotropy symmetry by Mitra *et al.* (2011).

4 CONCLUSIONS

(i) The result of the proposed DIRM measurement of Mitra *et al.* (2011) crucially depends on the initial state of the measured sample. Any sample can be prepared in a state with $IRAT = 1$ for all fields, namely the AF-demagnetized state in z -direction. It is therefore not possible that $IRAT$ directly reflects the symmetry of magnetic anisotropy.

(ii) Thermally demagnetized samples can show $IRAT$ values much lower than 1 if the applied field lies well within the range of the samples coercivity distribution, as measured, for example, by the FORC method. Especially pseudo-single domain and multidomain particles in real samples can display low $IRAT$ values.

(iii) The claimed dependence of $IRAT$ on the symmetry group, related to the magnetic anisotropy in ideal single domain ensembles may exist, but is overemphasized by the numerical model of Mitra *et al.* (2011).

(iv) The stated model result of $M_{rs}/M_s = 0.94$ for triaxial anisotropy in the basal plane contradicts analytical results for three dimensionally randomized platelets that yield an upper limit of 0.638.

(v) The observed trend in M_{rs}/M_s versus $IRAT$ for a set of MORB specimens across a chilled margin can alternatively be explained by varying coercivity and domain state in agreement with previous experiments (Gee & Kent 1995, 1999; Fabian 2003, 2006). Multiaxial magnetic anisotropy is not required for this explanation.

(vi) Conclusion (iii) of Mitra *et al.* (2011) claims the proof of multiaxial anisotropy for specimens near the chilled margin of this MORB sample. This is not correct, because no contradiction to a prevailing stress-induced uniaxial magnetic anisotropy is established by the ideas or data presented in their article.

ACKNOWLEDGMENTS

Thoughtful comments of two anonymous reviewers are gratefully acknowledged.

REFERENCES

Ambatiello, A. & Soffel, H.C., 1996. Kerr microscopy of small synthetic Ti-rich titanomagnetite grains, *Geophys. Res. Lett.*, **23**, 2807–2810.
 Bertotti, G., 1998. *Hysteresis in Magnetism*, Academic Press, San Diego.
 Bleil, U. & Petersen, N., 1983. Variation in magnetization intensity and low-temperature titanomagnetite oxidation of ocean floor basalts, *Nature*, **301**, 384–388.

Dunlop, D., 1969. Preisach diagrams and remanent properties of interacting monodomain grains, *Phil. Mag.*, **19**, 369–378.
 Dunlop, D.J., Westcott-Lewis, M.F. & Bailey, M.E., 1990. Preisach diagrams and anhysteresis: do they measure interactions? *Phys. Earth planet. Inter.*, **65**, 62–77.
 Fabian, K., 2003. Some additional parameters to estimate domain state from isothermal magnetization measurements, *Earth planet. Sci. Lett.*, **213**, 337–345.
 Fabian, K., 2006. Approach to saturation analysis of hysteresis measurements in rock magnetism and evidence for stress dominated magnetic anisotropy in young mid-ocean ridge basalt, *Phys. Earth planet. Inter.*, **154**, 299–307.
 Fabian, K. & von Dobeneck, T., 1997. Isothermal magnetization of samples with stable Preisach function: a survey of hysteresis, remanence and rock magnetic parameters, *J. geophys. Res.*, **102**, 17 659–17 677.
 Gee, J. & Kent, D.V., 1995. Magnetic hysteresis in young mid-ocean ridge basalts: dominant cubic anisotropy? *Geophys. Res. Lett.*, **22**, 551–554.
 Gee, J. & Kent, D.V., 1999. Calibration of magnetic granulometric trends in oceanic basalts, *Earth planet. Sci. Lett.*, **170**, 377–390.
 Girke, H., 1960. Der Einfluß innerer magnetischer Kopplungen auf die gestalt der Preisach-Funktionen hochpermeabler Materialien, *Z. Angew. Phys.*, **11**, 502–508.
 Hejda, P. & Zelinka, T., 1990. Modelling of hysteresis processes in magnetic rock samples using the Preisach diagram, *Phys. Earth planet. Inter.*, **63**, 32–40.
 Heslop, D., McIntosh, G. & Dekkers, M.J., 2004. Using time- and temperature-dependent Preisach models to investigate the limitations of modelling isothermal remanent magnetization acquisition curves with cumulative log Gaussian functions, *Geophys. J. Int.*, **157**, 55–63.
 Ivanov, V., Khaburzaniya, I.A. & Sholpo, L.Y., 1981. Use of Preisach diagrams for diagnosis of single- and multi-domain grains in rock samples, *Izv. Earth Phys.*, **17**, 36–43.
 Matzka, J., Krása, D., Kunzmann, T., Schult, A. & Petersen, N., 2003. Magnetic state of 10–40 Ma old ocean basalts and its implications for natural remanent magnetization, *Earth planet. Sci. Lett.*, **206**, 541–553.
 Mayergoyz, I.D., 1991. *Mathematical Models of Hysteresis*, Springer-Verlag, New York.
 Mitra, R., Tauxe, L. & Gee, J.S., 2011. Detecting uniaxial single domain grains with a modified IRM technique, *Geophys. J. Int.*, **187**, 1250–1258.
 Mullins, C. & Tite, M., 1973. Preisach diagrams and magnetic viscosity phenomena for soils and synthetic assemblies of iron oxide grains, *J. Geomag. Geoelectr.*, **25**, 213–229.
 Pike, C.R., Roberts, A.P. & Verosub, K.L., 1999. Characterizing interactions in fine magnetic particle systems using first order reversal curves, *J. appl. Phys.*, **85**(9), 6660–6667.
 Pike, C.R., Roberts, A.P., Dekkers, M.J. & Verosub, K.L., 2001. An investigation of multi-domain hysteresis mechanisms using FORC diagrams, *Phys. Earth planet. Inter.*, **126**(1–2), 11–25.
 Preisach, F., 1935. Über die magnetische Nachwirkung, *Z. Phys.*, **94**, 277–302.
 Visintin, A., 1991. *Differential Models of Hysteresis*, Springer-Verlag, Berlin.